crystals

MDPI

Article

Crystal Structure, Thermodynamic Properties and DFT Studies of 5,6-dimethyl-1H-benzo[d]imidazol-3-ium 3-((2,4-dioxo-1,5-dioxaspiro[5.5]undecan-3-ylidene)methyl) -2,4-dioxo-1,5-dioxaspiro[5.5]undecane Hydrate

Wulan Zeng [1,*], Xia Wang [1] and Yunju Zhang [2]

[1] Department of Chemistry, Chemical Engineering and Environmental Engineering, Weifang University, Weifang 261061, China; wangxia-2001@163.com
[2] Key Laboratory of Photoinduced Functional Materials, School of Chemistry and Chemical Engineering, Mianyang Normal University, Mianyang 621000, China; zhangyj010@nenu.edu.cn
* Correspondence: wulanzeng@163.com; Tel.: +86-536-8785802

Abstract: A new 1,5-dioxaspiro[5.5] derivative coupled with a benzimidazole moiety: 5,6-dimethyl-1H-benzo[d]imidazol-3-ium 3-((2,4-dioxo-1,5-dioxaspiro[5.5]undecan-3-ylidene) methyl) -2,4-dioxo-1,5-dioxaspiro[5.5]undecane hydrate (**DBH**) was prepared. The crystal structure confirmed that it belongs to triclinic, P-1 space group. The title compound includes one $(C_{19}H_{21}O_8)^-$ anion, one $(C_9H_{11}N_2)^+$ cation and one water molecule, which assembled into a 2D-net framework by O–H···O and N–H···O hydrogen bonds. The quantum chemical computations using the B3LYP/6-311G (d, p) basis level of theory reveal that the optimized geometric structure is suitable to study the molecule. The theoretically simulated FT-IR spectra and electronic spectra of **DBH** are compared with experimental data. The results show that the B3LYP/6-311g (d, p) method fits well with the molecular structure. In addition, the thermodynamic properties have also been studied to determine the nature of the **DBH**.

Keywords: 5,6-dimethyl-1H-benzo[d]imidazole; crystal structure; DFT calculation; vibrational frequencies; thermodynamic properties

check for updates

Citation: Zeng, W.; Wang, X.; Zhang, Y. Crystal Structure, Thermodynamic Properties and DFT Studies of 5,6-dimethyl-1H-benzo[d]imidazol-3-ium 3-((2,4-dioxo-1,5-dioxaspiro[5.5] undecan-3-ylidene)methyl) -2,4-dioxo-1,5-dioxaspiro[5.5]undecane Hydrate. *Crystals* **2021**, *11*, 1393. https://doi.org/10.3390/cryst11111393

Academic Editors: Alexander Y. Nazarenko and Kil Sik Min

Received: 23 October 2021
Accepted: 12 November 2021
Published: 15 November 2021

Publisher's Note: MDPI stays neutral with regard to jurisdictional claims in published maps and institutional affiliations.

1. Introduction

Heterocyclic compounds play an important role in biochemistry, medicinal chemistry, organic chemistry and agrochemical industries. In recent years, attention has been given to the benzimidazole class of compounds due to their diverse biological activities, such as anticancer [1,2], antifungal [3], antioxidant [4], cytotoxic [5], antiprotozoal [6], anti-T. cruzi (Trypanosoma cruzi) [7], antiproliferative [8], antihistaminic [9], anti-inflammatory [10], analgesics [11], antibacterial [12], anticonvulsant [13] and acetylcholinesterase [14]. In addition, benzimidazole has been used as corrosion inhibition for mild steel [15], catalytic activity [16], fluorescence chemosensors [17] and chiroptical sensors [18]. As other heterocyclic compounds, spiro compounds containing O heteroatom have also attracted much attention due to its special structure in recent years. All kinds of spirocyclic compounds were designed and synthesized [19–21]. Based on the above reasons, our group has prepared several spirocyclic compounds derived from the 1,5-dioxaspiro group or the 6,10-dioxaspiro group in ten years [22–25]. However, to the best of our knowledge, among so many reported oxaspirocyclic compounds, neither theory studies nor comparison between the experimental and calculational results for derivatives from a benzodimidazole moiety are available. Herein, we have prepared a new 1,5-dioxaspiro[5.5] derivative coupled with benzodimidazole moiety: 5,6-dimethyl-1H-benzo[d]imidazol-3-ium 3-((2,4-dioxo-1,5-dioxaspiro[5.5]undecane-3-ylidene)methyl)-2,4-dioxo-1,5-dioxaspiro[5.5] unde-

cane hydrate (**DBH**), seen as Scheme 1. In addition, its crystal structure, FT-IR spectra and electronic spectra have been compared with DFT or TD-DFT calculational results.

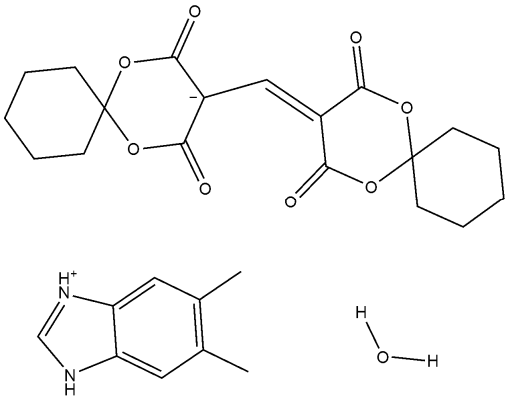

Scheme 1. The molecular structure of **DBH.**

2. Materials and Methods

2.1. Physical Measurements

The infrared (IR) spectra were recorded using a Nicolet 6700 spectrometer (Nicolet Instrument Inc., Madison, WI, USA). The C, H, and N elemental analyses were performed on an Elementar Vario EL III elemental analyzer (Elementar, Hanau, Germany). The UV–Vis spectra were measured on a TU-1901 spectrometer (Persee, Beijing, China). ^{1}H NMR and ^{13}C NMR spectra were obtained with a Bruker AVANCE III HD NMR (400 MHz) spectrometer (Bruker, Elisabethhof, The Netherlands) in $CDCl_3$.

2.2. Preparation of DBH

The trimethyl orthoformate (1.27 g, 12 mmol) was refluxed with 1,5-dioxaspiro[5.5]undecane-2,4-dione (1.84 g, 10 mmol) in ethanol (30 mL) for 3 h at 60 °C. After adding 5,6-dimethyl-1H-benzene (1.46 g, 10mmol), the mixture lasted for a further 4 h. Then, the above mixture was cooled, and the yellow powder (**DBH**) was isolated by filtration. Yield 17.8 %. m. p.: 175.2–175.3 °C. Anal. Calcd. for C_{28} H_{34} N_2 O_9: C, 61.98; H, 6.32; N, 5.16. Found: C, 61.83; H, 6.27; N, 5.25. ^{1}H NMR (400 MHz, $CDCl_3$, δ_{ppm}) 9.55 (s, 1H), 8.80 (s, 1H), 7.53 (s, 1H), 4.37 (m, 3H), 2.36 (s, 6H), 2.01 (t, J = 8.0 Hz, 8H), 1.56 (s, 2H), 1.44 (m, 6H), 1.34 (m, 6H). ^{13}C NMR (125 MHz, $CDCl_3$, δ_{ppm}) 151, 138, 134, 132, 114,103, 95, 34, 24, 23, 20. Yellow block crystals are obtained using ethanol solvents.

2.3. X-ray Diffraction Analysis of DBH

The crystal of **DBH** was mounted on a Spider Rapid IP (Rigaku, Japan) area detector at 293 K. Reflection data were obtained using MoKα (λ = 0.71073 Å) radiation. Its structure was solved using SHELXL-2015 and SHELXT-2015 [26,27], respectively. The H atoms of **DBH** were refined using the riding model. The final *R* indices: R_1 = 0.045, wR_2 = 0.1099 for 4741 reflections with I > 2σ(I) using the weighting scheme, $w = 1/[\sigma^2(Fo^2) + (0.645\ P)^2 + 0.1579P]$, where $P = (Fo^2 + 2Fc^2)/3$.

2.4. Computational Methods

The Gaussian 09 [28] software is used to execute the quantum chemical computations by the DFT/B3LYP method with a 6-311G (d, p) basis set [29]. Gauss view is used to inspect the output graphically obtained by the Gaussian 09 software. The geometric optimization of **DBH** is accomplished by DFT/B3LYP/6-311G (d, p) level of theory [30]. The FT-IR infrared and electronic spectra are calculated by the same method. The calculated wavenumbers are scaled by 0.96 at the B3LYP/6-311G (d, p) level.

3. Results and Discussion

*3.1. Crystal Structure of **DBH***

The crystal data and structure refinement for **DBH** are list in Table 1. Its molecular structure, which includes no H atoms, and its optimized geometric structure are both shown in Figure 1.

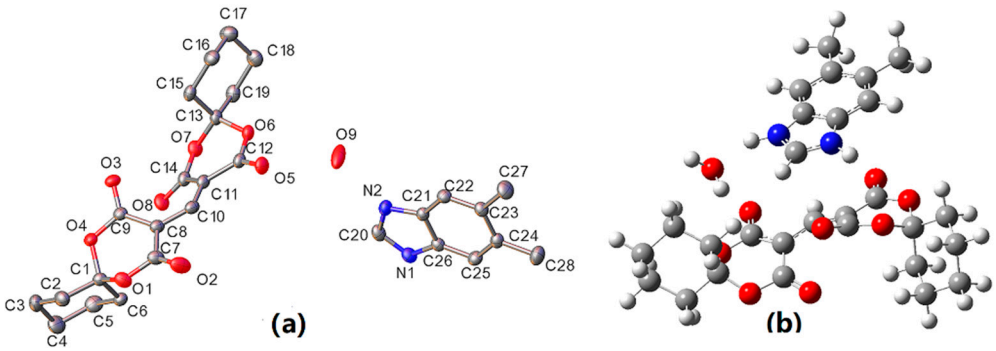

Figure 1. (**a**) ORTEP drawings of **DBH**; (**b**) optimized geometric structure of **DBH**.

Table 1. Crystal Data and Structure Refinement for **DBH.**

Formula	$C_{28}H_{34}N_2O_9$
CCDC	1948628
Mr	380.35
Color/shape	yellow/block
Temperature	293(2) K
Crystal system, space group	Triclinic, P-1
Unit cell dimensions	a = 10.5431(3) Å α = 73.9160(10)° b = 11.3397(4) Å β = 70.7600(10)° c = 12.4926(4) Å γ =89.8030(10)°
V	1348.57(8) Å^3
Z, Density	2, 1.336 Mg/m^3
μ	0.100 mm^{-1}
F(000)	576
θ	3.117 to 27.484°
Limiting indices	$-13 \leq h \leq 12$, $-14 \leq k \leq 14$, $-16 \leq l \leq 16$
No. of reflections collected/unique	13,425/6145 (R_{int} = 0.0188)
No. of parameters	357
GOF	1.132
R_1 ($I > 2\sigma$ (I))	0.0450
wR_2 ($I > 2\sigma$ (I))	0.1099
R_1 (all data)	0.0595
wR_2 (all data)	0.1284
Largest diff. peak and hole	0.372 and −0.224 e. Å^{-3}

As shown in Figure 1 and Table 2, **DBH** is composed of one $(C_{19}H_{21}O_8)^-$ anion, one $(C_9H_{11}N_2)^+$ cation and one water molecule. The central C(10) atom is used to join two 1,5-dioxaspiro[5.5] undecane-2,4-dione moieties. The bond lengths reported for C8–C10 and C10–C11 are 1.389(2) Å and 1.382(2) Å, respectively, which resemble related published compounds (1.386(2) Å, 1.380(2) Å) [24]. Their corresponding calculated results are 1.395 Å and 1.388 Å. On the other hand, the bond angle of C8–C10–C11 in predicted values with the experimental ones is 132.30° and 130.62(13)°, respectively, which is also similar to related structures reported(C15–C17–C9 131.19(1)°) [24]. The experimental torsion angles for C7–C8–C10–C11, C8–C10–C11–C12, C8–C10–C11–C14 and C9–C8–C10–C11 are 167.64(14)°, 168.36(13)°, −20.60(2)° and −21.40(2)°, respectively. Their corresponding calculated torsion angles are 168.64°, 166.71°, −24.00°, and −24.28°, respectively. The two 1.3-dioxane rings R1 (O1, C1, O4, C9, C8, C7) and R2 (O6, C12, C11, C14, O7, C13) display distorted envelope

conformation, with puckering parameters (Q, ϑ, φ) of (0.5052 Å, 105.63°, 234.40°) and (0.4781 Å, 70.33°, 304.46°), respectively. The maximum difference of bond lengths, bond angles and torsion angles between experimental values and calculated ones is 0.019 Å, 1.68° and 3.4°, respectively, which hereby certifies that the B3LYP/6-311G (d, p) level can simulate the crystal structure.

Table 2. Experimental and Computational Bond Distances (Å), Bond Angles (°) and Torsion Angles for **DBH**.

Bond Lengths	**Exp. (Å)**	**Calc. (Å)**	**Bond**	**Exp. (Å)**	**Calc. (Å)**
C8–C10	1.389(2)	1.395	O1–C1	1.436(16)	1.419
C10–C11	1.382(2)	1.388	O1–C7	1.365(18)	1.385
O8–C14	1.213(16)	1.201	C1–O4	1.441(15)	1.449
O5–C12	1.212(16)	1.231	O2–C7	1.218(17)	1.201
O6–C12	1.361(17)	1.351	O3–C9	1.221(16)	1.231
O6–C13	1.438 (15)	1.456	O4–C9	1.356(16)	1.352
O7–C14	1.363(18)	1.382	N1–C20	1.318(2)	1.329
N2–C20	1.322(19)	1.333	N2–C21	1.389(17)	1.391
Bond angle	Exp (°)	Calc. (°)	Bond angle	Exp (°)	Calc. (°)
C11–C10–C8	130.62(13)	132.30	C10–C8–C7	118.45(13)	117.36
C10–C11–C12	117.58(12)	117.45	C10–C8–C9	123.96(12)	123.18
C10–C11–C14	123.67(12)	122.91	C7–C8–C9	117.00(13)	118.61
C12–C11–C14	118.17(13)	118.41	N1–C20–N2	110.32(12)	110.43
Torsion angle	Exp (°)	Calc. (°)	Torsion angle	Exp (°)	Calc. (°)
C7–C8–C10–C11	167.64(14)	168.64	O1–C7–C8–C9	19.52(18)	18.90
C8–C10–C11–C12	168.36(13)	166.71	O2–C7–C8–C9	−158.30(15)	−160.69
C8–C10–C11–C14	−20.6(2)	−24.00	C9–C8–C10–C11	−21.4(2)	−24.28

In **DBH**, the H_2O molecule connects the two $(C_{19}H_{21}O_8)^-$ anions with the $(C_9H_{11}N_2)^+$ cation via O9–H9A···O2, O9–H9B···O5 hydrogen bonds and N2–H2···O9 hydrogen bonds, respectively. The distance of O9···O2, O9···O5 and N2···O9 is 2.792(18) Å, 2.728(16) Å and 2.650(18) Å, respectively (Table 3). The $(C_9H_{11}N_2)^+$ cation and the $(C_{19}H_{21}O_8)^-$ anion were linked by N1–H1···O3 intermolecular hydrogen bonds, and donor and acceptor distances are 2.777(15) Å, symmetry code: x, y − 1, z. **DBH** displays a 2D-net structure by O–H···O and N–H···O hydrogen bonds (Figure 2). A three-dimensional network was further generated by the above hydrogen bonds, as shown in Figure 3.

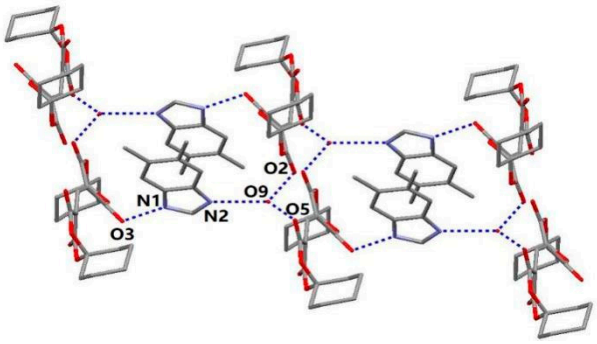

Figure 2. 2D-net structure of **DBH.**

Table 3. N–H···O and O–H···O Molecular Interactions for **DBH**.

D–H···A	**Symmetry**	**D–H (Å)**	**H···A (Å)**	**D···A (Å)**	**∠D–H···A (°)**
N1–H1···O3	x, y − 1, z	0.86	1.94	2.777 (15)	165.0
N2−H2···O9	intra	0.86	1.79	2.650(18)	172.3
O9–H9A···O2	−x + 2, −y + 1, z + 1	0.86	1.97	2.792(18)	161.6
O9–H9B···O5	intra	0.86	1.90	2.728(16)	165.5

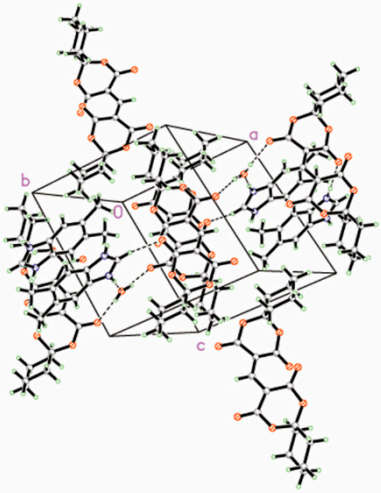

Figure 3. Packing diagram of **DBH** with 30% probability thermal ellipsoids.

3.2. Vibrational Analysis

As shown in Figure 4, the ν_{O-H} vibration appeared at 3383 cm^{-1} in the infrared spectra and at 3388 cm^{-1} in DFT calculations, which is due to the water of **DBH**. The ν_{C-H} vibration of the 5,6-dimethyl-1H-benzo[d]imidazole ring appeared at 3106 cm^{-1}, and the corresponding calculated band was observed at 3126 cm^{-1}. The calculated and experimental $\nu_{C=O}$ vibrations of the 1,3-dioxane ring were observed at 1737 cm^{-1} and 1629 cm^{-1} and at 1691 cm^{-1} and 1652 cm^{-1}, respectively. The ν_{C-O} bands of 1,3-dioxane ring were seen at 1261 cm^{-1} and 1225 cm^{-1} in DFT and at 1255 cm^{-1} and 1215 cm^{-1} in the IR spectra, respectively. These values agree well with literature reports [22–24]. The $\nu_{C=N}$ and ν_{C-N} vibrations occurred at 1490 cm^{-1} and 1347 cm^{-1} in DFT, respectively. The corresponding bands were seen at 1489 cm^{-1} and 1366 cm^{-1} in the IR spectra. In a word, the IR spectra for **DBH** agree very well with the calculated values.

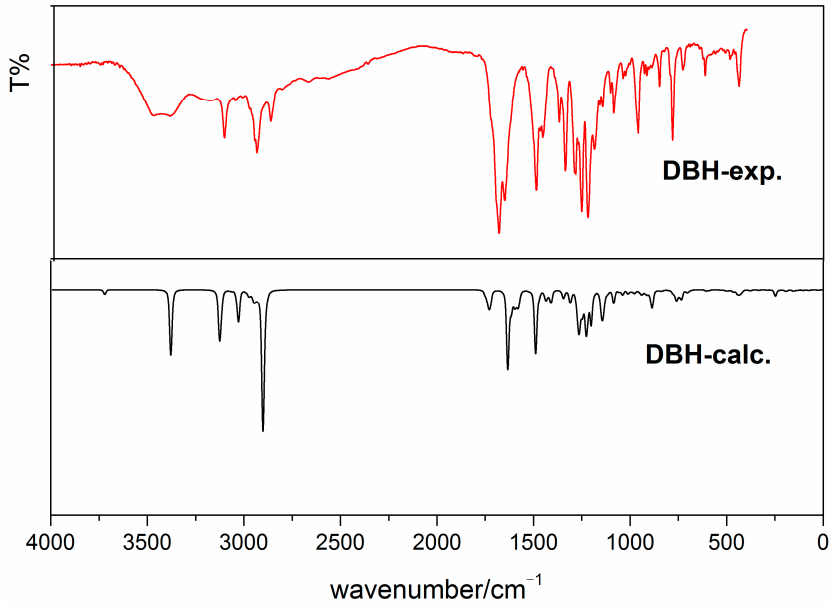

Figure 4. Experimental and calculated IR spectra of **DBH**.

3.3. Thermodynamic Properties

Thermodynamic parameters for different temperatures were calculated at the B3LYP/6-311G (d, p) level and scaled by 0.96. Three main thermodynamic properties—capacity ($C^0_{p,m}$), entropy (S^0_m) and enthalpy (H^0_m)—are listed in Table 4. As shown in Table 4, all

the values increase when the temperature rises in the range of 100.0–1000.0 K, which is mainly because a higher temperature can strengthen the vibration of molecules [31].

The correlation equations of $C^0{}_{p,m}$, $S^0{}_m$, $H^0{}_m$ and temperature T are as follows:

$$C^0{}_{p,m} = 15.072 + 2.275\,T - 9.247{*}10^{-4}\,T^2\ (R^2 = 0.99947)$$

$$S^0{}_m = 293.009 + 2.345\,T - 4.947{*}10^{-4}\,T^2\ (R^2 = 0.99999)$$

$$H^0{}_m = -26.153 + 0.249\,T + 6.323{*}10^{-4}\,T^2\ (R^2 = 0.9994)$$

Table 4. $C^0{}_{p,m}$, $S^0{}_m$ and $H^0{}_m$ from 100.0 to 1000.0 K at the B3LYP/6-311G (d, p) level.

T (K)	$C^0{}_{p,m}$ (J·mol^{-1}·K^{-1})	$S^0{}_m$ (J·mol^{-1}·K^{-1})	$H^0{}_m$ (kJ·mol^{-1})
100.0	245.91	520.42	14.32
200.0	423.94	745.99	47.88
298.1	601.87	948.26	98.18
300.0	605.24	951.99	99.29
400.0	780.04	1150.47	168.70
500.0	930.87	1341.24	254.48
600.0	1054.72	1522.29	353.97
700.0	1155.81	1692.73	464.66
800.0	1239.14	1852.68	584.54
900.0	1308.68	2002.76	712.03
1000.0	1367.29	2143.76	845.91

3.4. Electronic Analysis

To compare with the experimental spectra, the calculated spectra of **DBH** are performed with the TD-DFT/B3LYP/6-311G (d, p) basis level and shown in Figure 5. As seen in Figure 5, two peaks arise at 245 nm and 378 nm in the experimental spectra and 252 nm and 339 nm in the calculated spectra, respectively. Figure 6 depicts eight frontier molecular orbitals of **DBH**, which is in agreement with the electron transitions shown in Table 5. As shown in Figure 6, the electron clouds of **DBH** are mainly localized on 5,6-dimethyl-1H-benzo[d]imidazole ring, two 1,3-dioxane rings and C8–C10=C11 bands, which indicate that the electronic transitions in UV–Vis spectra are in accordance with $\pi \rightarrow \pi^*$ and $n \rightarrow \pi^*$ transitions. For example, the first peak at 252 nm is mainly assigned to three electronic transition modes HOMO-5→LUMO+2, HOMO-4→LUMO and HOMO-3→LUMO. In HOMO-5, HOMO-4 and HOMO-3, electrons are distributed on the 5, 6-dimethyl-1H-benzo[d]imidazole ring, two 1,3-dioxane rings and C8–C10=C11 bonds, while in LUMO and LUMO+2, electrons are distributed on the 5, 6-dimethyl-1H-benzo[d]imidazole ring. The second peak at 339 nm is only one electronic transition mode HOMO→LUMO+1. In HOMO and LUMO+1, electrons are distributed on both two 1,3-dioxane rings and C8–C10=C11 bonds. Then, electronic transitions related with the peak at 339 nm are mainly from C8–C10=C11 bonds and oxygen atoms of 1,3-dioxane rings to C8–C10=C11 bonds, which are consistent with $\pi \rightarrow \pi^*$ and $n \rightarrow \pi^*$ transitions [32].

Table 5. Experimental and calculated electronic absorption spectra values.

Exp.	Calc. (TD-DFT)		
Wavelength (nm)	**Wavelength (nm)**	**Oscillator Strength(f)**	**Electronic Transition Modes**
245	252	0.2079	139HOMO − 5→147LUMO + 2 140HOMO − 4→145LUMO 141HOMO − 3→145LUMO
378	339	0.4089	144HOMO→146LUMO + 1

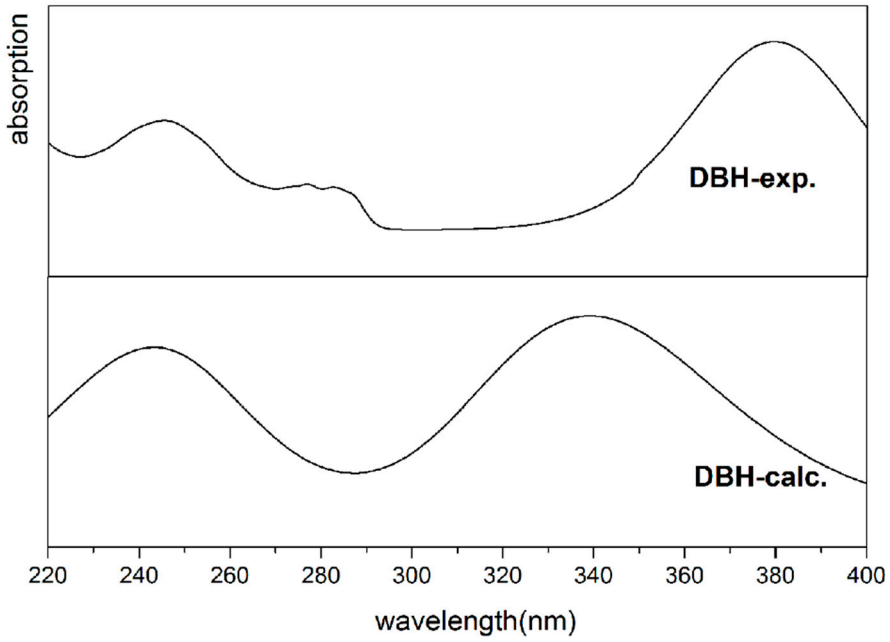

Figure 5. Experimental and calculated UV–Vis spectra of **DBH**.

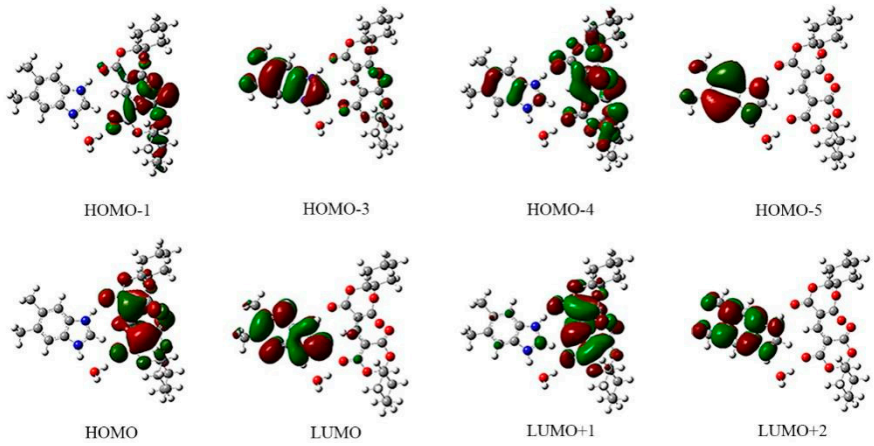

Figure 6. The eight frontier molecular orbitals of **DBH**.

4. Conclusions

5,6-dimethyl-1H-benzo[d]imidazol-3-ium,3-((2,4-dioxo-1,5-dioxaspiro[5.5]undecan-3-ylidene)methyl)-2,4-dioxo-1,5-dioxaspiro[5.5]undecane hydrate (**DBH**) has been prepared, and its structure has been confirmed by single-crystal X-ray diffraction. **DBH** includes one $(C_{19}H_{21}O_8)^-$ anion, one $(C_9H_{11}N_2)^+$ cation and one water molecule, which assembled into a 2D-net framework by O–H···O and N–H···O hydrogen bonds. By comparing with experimental values, the calculated vibration frequencies and electronic spectra of **DBH** using the DFT/B3LYP/6-311g (d, p) level of theory fit well with the molecule.

Author Contributions: W.Z. designed the experiment and wrote the paper. X.W. synthesized the title compound (**DBH**) and provided the funds. Y.Z. calculated the vibration spectra and electronic spectra. All authors have read and agreed to the published version of the manuscript.

Funding: This research was funded by the National Natural Science Foundation of China (No. 22108208) and the State Key Laboratory of High-efficiency Utilization of Coal and Green Chemical Engineering (No. 2021-K02).

Data Availability Statement: CCDC 1948628 (**DBH**) contains the supplementary crystallographic data for this paper. These data can be obtained free of charge at www.ccdc.cam.ac.uk/conts/retrieving.html, accessed on 23 October 2021, or from the Cambridge CrystallographicData Centre (CCDC), 12 Union Road, Cambridge CB2 1EZ, UK; fax: +44(0)1222-336033; email: deposit@ccdc.cam.ac.uk.

Conflicts of Interest: The authors declare no competing financial interest.

References

1. Haoran, W.; Akhtar, W.; Nainwal, L.M.; Kaushik, S.K.; Akhter, M.; Shaquiquzzaman, M.; Alam, M.M. Synthesis and biological evaluation of benzimidazole pendant cyanopyrimidine derivatives as anticancer agents. *J. Heterocycl. Chem.* **2020**, *57*, 3350–3360. [CrossRef]
2. Natha, J.; Paul, R.; Ghosh, S.K.; Paul, J.; Singha, B.; Debnath, N. Drug repurposing and relabeling for cancer therapy: Emerging benzimidazole antihelminthics with potent anticancer effects. *Life Sci.* **2020**, *258*, 118189. [CrossRef] [PubMed]
3. Ansari, K.F.; Lal, C. Synthesis, physicochemical properties and antimicrobial activity of some new benzimidazole derivatives. *Eur. J. Med. Chem.* **2009**, *44*, 4028–4033. [CrossRef] [PubMed]
4. Bektas, H.; Sökmen, B.B.; Aydın, S.; Menteşe, E.; Bektaş, A.; Dilekçi, G. Design, synthesis, and characterization of some new benzimidazole derivatives and biological evaluation. *J. Heterocycl. Chem.* **2020**, *57*, 2234–2242. [CrossRef]
5. Khalifa, M.E. Synthesis and evaluation of new 2-mercaptomethyl benzimidazole scaffolds as potential antibacterial, antioxidant and cytotoxic agents. *ChemistrySelect* **2020**, *5*, 10562–10566. [CrossRef]
6. Flores-Carrillo, P.; Velázquez-López, J.M.; Aguayo-Ortiza, R.; Hernández-Campos, A.; Trejo-Soto, J.; Yépez-Mulia, L.; Castillo, R. Synthesis, antiprotozoal activity, and chemoinformatic analysis of 2-(methylthio)-1H-benzimidazole-5-carboxamide derivatives: Identification of new selective. *Eur. J. Med. Chem.* **2017**, *137*, 211–220. [CrossRef]
7. Beltran-Hortelano, I.; Alcolea, V.; Font, M.R.; Pérez-Silanes, S. The role of imidazole and benzimidazole heterocycles in Chagas disease: A review. *Eur. J. Med. Chem.* **2020**, *206*, 112692. [CrossRef] [PubMed]
8. Akkoça, S.; Tüzün, B.; İlhan, I.Ö.; Akkurt, M. Efficient synthesis and molecular docking studies of new pyrimidine-chromeno hybrid derivatives as potential antiproliferative agents. *J. Mol. Struct.* **2020**, *1219*, 128582.
9. Caymaz, B.; Yıldız, U.; Akkoç, S.; Gerçek, Z.; Şengül, A. Synthesis, characterization, and antiproliferative activity studies of novel benzimidazole-Imidazopyridine hybrids as DNA groove binders. *ChemistrySelect* **2020**, *5*, 8465–8474. [CrossRef]
10. Agliano, F.; Karlinsey, K.S.; Ragazzi, M.; Ménoret, A.; Vella, A.T. A benzimidazole inhibitor attenuates sterile inflammation induced in a model of systemic autoinflammation in female mice. *Sci. Rep.* **2020**, *10*, 12100. [CrossRef] [PubMed]
11. Sondhi, S.M.; Rajvanshi, S.; Johar, M.; Bharti, N.; Azam, A.; Singh, A.K. Anti-inflammatory, analgesic and antiamoebic activity evaluation of pyrimido[1,6-a]benzimidazole derivatives synthesized by the reaction of ketoisothiocyanates with mono and diamines. *Eur. J. Med. Chem.* **2002**, *37*, 835–843. [CrossRef]
12. Zeynep, A.A. Antimicrobial Activities of 1-H-Benzimidazole-based Molecules. *Curr. Top. Med. Chem.* **2016**, *16*, 2953–2962.
13. Vasil'ev, P.M.; Kalitin, K.Y.; Spasov, A.A.; Grechko, O.Y.; Poroikov, V.V.; Filimonov, V.V.; Anisimova, V.A. Prediction and study of anticonvulsant properties of benzimidazole derivatives. *Pharm. Chem. J.* **2017**, *50*, 775–780. [CrossRef]
14. Alpan, A.S.; Parlar, S.; Carlino, L.; Tarikogullari, A.H.; Alptüzün, V.; Günes, H.S. Synthesis, biological activity and molecular modeling studies on 1H-benzimidazole derivatives as acetylcholinesterase inhibitors. *Bioorg. Med. Chem.* **2013**, *21*, 4928–4937. [CrossRef]
15. Chaouiki, A.; Chafiq, M.; Rbaa, M.; Salghi, R.; Lakhrissi, B.; Ali, I.H.; Bashir, S.; Chung, I.M.J. Comprehensive assessment of corrosion inhibition mechanisms of novel benzimidazole compounds for mild steel in HCl: An experimental and theoretical investigation. *J. Mol. Liq.* **2020**, *320*, 114383. [CrossRef]
16. Allahresani, A.; Naghdi, E.; Nasseri, M.A. Catalytic activity of Co (II) Salen@ KCC-1 on the synthesis of 2, 4, 5-triphenyl-1H-imidazoles and benzimidazoles. *Inorg. Chem. Commun.* **2020**, *119*, 108137. [CrossRef]
17. Maji, A.; Pal, S.; Lohar, S.; Mukhopadhyay, S.K.; Chattopadhyay, P. A new turn-on benzimidazole-based greenish-yellow fluorescent sensor for Zn 2+ ions at biological pH applicable in cell imaging. *New J. Chem.* **2017**, *41*, 7583–7590. [CrossRef]
18. John, M.E.; Karnik, A.V. Chiral benzimidazole derived bis-phenyl triazoles as chiroptical sensors for iodide and chiral amines. *J. Heterocycl. Chem.* **2020**, *57*, 2844–2853. [CrossRef]
19. Ramachary, D.B.; Krishna, P.M. Asymmetric synthesis of nature-inspired bioactive spiro compounds through organocatalytic diels–alder reactions. *Asian J. Org. Chem.* **2016**, *5*, 729–734. [CrossRef]
20. Niu, Q.; Xi, J.; Li, L.; Li, L.; Pan, C.; Lan, M.; Ronget, L. Isatins 3-C annulation vs ring-opening: Two different pathways for synthesis of spiro compounds via multicomponent reactions. *Tetrahedron Lett.* **2019**, *60*, 151181. [CrossRef]
21. Guo, C.; Li, B.; Liu, H.; Zhang, X.; Zhang, X.; Fan, X. Synthesis of fused or spiro polyheterocyclic compounds via the dehydrogenative annulation reactions of 2-arylindazoles with maleimides. *Org. Lett.* **2019**, *21*, 7189–7193. [CrossRef]
22. Zeng, W.; Wang, X. Crystal structures of spiro derivatives including 6,10-dioxaspiro[4.5] decane-7,9-dione group and their spectral studies. *J. Chem. Crystallogr.* **2019**, *49*, 139–145. [CrossRef]
23. Zeng, W.; Jiang, J.; Jiang, G.; Li, Y. Synthesis, characterization, and fluorescence properties of two new heterocyclic compounds containing 1,5-dioxaspiro group. *Crystals* **2018**, *8*, 269. [CrossRef]
24. Zeng, W.; Jiang, J. Synthesis and crystal structure of a new hydrated benzimidazolium salt containing spiro structure. *Crystals* **2017**, *7*, 303. [CrossRef]

25. Zhang, Y.; Zeng, W. The crystal structure of 8-((4-chlorophenylamino) methylene)-6,10-dioxaspiro[4.5]decane-7,9-dione, C15H14ClNO4. *Kristallogr. NCS* **2020**, *235*, 925–927. [CrossRef]
26. Sheldrick, G.M. Crystal structure refinement with SHELXL. *Acta Crystallogr. Sect. C Cryst. Struct. Commun.* **2015**, *71*, 3–8. [CrossRef] [PubMed]
27. Sheldrick, G.M. SHELXT–Integrated space-group and crystal-structure determination. *Acta Crystallogr. Sect A* **2015**, *71*, 3–8. [CrossRef] [PubMed]
28. Frisch, M.J.; Trucks, G.W.; Schlegel, H.B.; Scuseria, G.E.; Robb, M.A.; Cheeseman, J.R.; Scalmani, G.; Barone, V.; Mennucci, B.; Petersson, G.A.; et al. Gaussian, Inc. Wallingford CT. 2013. Available online: https://gaussian.com/citation/ (accessed on 13 October 2021).
29. Scalmani, G.; Frisch, M.J.; Mennucci, B.; Tomasi, J.; Cammi, R.; Barone, V. Geometries and properties of excited states in the gas phase and in solution: Theory and application of a time-dependent density functional theory polarizable continuum model. *J. Chem. Phys.* **2006**, *124*, 094107. [CrossRef]
30. Bauernschmitt, R.; Ahlrichs, R. Treatment of electronic excitations within the adiabatic approximation of time dependent density functional theory. *Chem. Phys. Lett.* **1996**, *256*, 454–464. [CrossRef]
31. Khemalapure, S.S.; Hiremath, S.M.; Hiremath, C.S.; Kattia, V.S.; Basanagouda, M. Structural, spectroscopic and computational investigations on (4,6-dimethyl-benzofuran-3-yl)-acetic acid hydrazide. *J. Mol. Struct.* **2020**, *1220*, 128748. [CrossRef]
32. Zhao, P.; Gao, X.; Song, J.; Sun, X.; Zeng, W.L. Synthesis, characterization, crystal structure and DFT studies on 3-(1H-benzo[d][1,2,3]triazol-1-yl)-1-oxo-1-m-tolylpropan-2-yl-nicotinate. *Spectrochim. Acta Part A* **2011**, *79*, 219–225. [CrossRef] [PubMed]